Title

Exposure to Dimethyl Selenide (DMSe)-Derived Secondary Organic Aerosol Alters Transcriptomic Profiles in Human Airway Epithelial Cells

Journal

Environmental Science and Technology, 53(24)

ISSN

0013-936X

Authors

Ahmed, CM Sabbir
Cui, Yumeng
Frie, Alexander L
et al.

Publication Date

2019-12-17

DOI

10.1021/acs.est.9b04376

Peer reviewed

HHS Public Access

Author manuscript

Environ Sci Technol. Author manuscript; available in PMC 2020 December 17.

Published in final edited form as:

Environ Sci Technol. 2019 December 17; 53(24): 14660–14669. doi:10.1021/acs.est.9b04376.

Exposure to Dimethyl Selenide (DMSe)-Derived Secondary Organic Aerosol Alters Transcriptomic Profiles in Human Airway Epithelial Cells

C. M. Sabbir Ahmed[†], **Yumeng Cui**[‡], **Alexander L. Frie**[‡], **Abigail Burr**[§], **Rohan Kamath**[§], **Jin Y. Chen**[†], **Arafat Rahman**[‖], **Tara M. Nordgren**[†,§], **Ying-Hsuan Lin**[*,†,‡], **Roya Bahreini**[*,†,‡]

[†]Environmental Toxicology Graduate Program, University of California, Riverside, California 92521, United States

[‡]Department of Environmental Sciences, University of California, Riverside, California 92521, United States

[§]Division of Biomedical Sciences, University of California, Riverside, California 92521, United States

[‖]Genetics, Genomics, and Bioinformatics, University of California, Riverside, California 92521, United States

Abstract

Dimethyl selenide (DMSe) is one of the major volatile organoselenium compounds released from aquatic and terrestrial environments through microbial transformation and plant metabolism. The detailed processes of DMSe leading to secondary organic aerosol (SOA) formation and the pulmonary health effects induced by inhalation of DMSe-derived SOA remain largely unknown. In this study, we characterized the chemical composition and formation yields of SOA produced from the oxidation of DMSe with OH radicals and O_3 in controlled chamber experiments. Further, we profiled the transcriptome-wide gene expression changes in human airway epithelial cells (BEAS-2B) after exposure to DMSe-derived SOA. Our analyses indicated a significantly higher SOA yield resulting from the OH-initiated oxidation of DMSe. The oxidative potential of DMSe-derived SOA, as measured by the dithiothreitol (DTT) assay, suggested the presence of oxidizing moieties in DMSe-derived SOA at levels higher than typical ambient aerosols. Utilizing RNA sequencing (RNA-Seq) techniques, gene expression profiling followed by pathway enrichment

[*]**Corresponding Authors:** Ying-Hsuan.Lin@ucr.edu. Phone: +1-951-827-3785(Y.-H.L.). Roya.Bahreini@ucr.edu. Phone: +1-951-827-4506 (R.B.).

Supporting Information

The Supporting Information is available free of charge at https://pubs.acs.org/doi/10.1021/acs.est.9b04376.

Description of cytotoxicity assay; summary of smog chamber experimental conditions (Table S1); alignment rates of samples with the human reference genome (hg19) (Table S2); and list of the perturbed pathways in BEAS-2B cells exposed to DMSe-derived SOA (Tables S3 and S4); pipeline for RNA-Seq analysis (Figure S1); list of identified DEGs related to oxidative stress, ROS generation or antioxidant enzymes at the cellular level (Figure S2); the relative expression of highlighted genes in the discussion (Figure S3); time trend of the ratio of common nitrate ions during DMSe oxidation experiments in comparison with the ratio observed during ammonium nitrate calibrations (Figure S4); DTT activity (pmol μg min^{-1}) for both frozen and fresh SOA samples from OH and O_3 oxidations of DMSe (Figure S5); cytotoxicity induced by extracts of DMSe-derived SOA from O_3 and OH oxidations (Figure S6); and number of common and unique DEGs induced by SOA generated by O_3 and OH oxidation products (Figure S7) (PDF)

The authors declare no competing financial interest.

analysis revealed several major biological pathways perturbed by DMSe-derived SOA, including elevated genotoxicity, DNA damage, and p53-mediated stress responses, as well as downregulated cholesterol biosynthesis, glycolysis, and interleukin IL-4/IL-13 signaling. This study highlights the significance of DMSe-derived SOA as a stressor in human airway epithelial cells.

Graphical Abstract

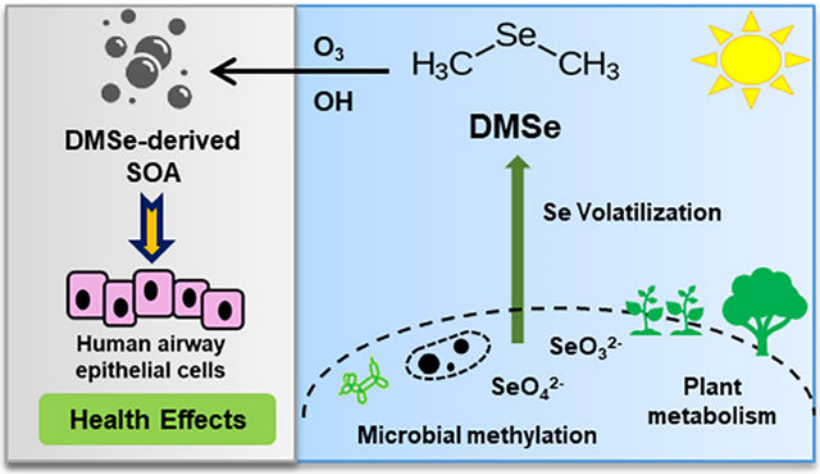

1. INTRODUCTION

Selenium (Se) is a trace element existing in natural environments and also a micronutrient essential for human health.[1,2] The oxidation states of Se are critical to determining its solubility, mobility, bioavailability, and toxicity.[3] The average Se concentration in soils is ~0.4 mg kg^{-1}, with elevated levels of up to 5000 mg kg^{-1} in certain regions including the United States, Canada, China, Japan, Venezuela, and India.[1] The occurrence of Se in these regions depends upon the type of soil, extent of soil erosion, organic matter, and rainfall. In addition, the elevated Se levels can be associated with the overuse of Se-containing fertilizers.[1,3] Atmospheric deposition and soil drainage make Se available in water bodies.[1,2] In underground water, Se concentrations increase due to the use of Se-containing fertilizers in agricultural lands.[3] Oxyanions of Se^{4+} and Se^{6+} along with a number of selenides (Se^{2-}) are predominately present in aquatic environments.[4] A significant transitory reservoir for Se element is the air.[4,5] Microbial transformation in both terrestrial and aquatic systems contributes to the volatilization of Se and its release into the atmosphere in methylated forms, such as dimethyl selenide (DMSe), dimethyl diselenide (DMDSe), methaneselenol, or the inorganic selenium dioxide (SeO_2). The presence of volatile DMSe has been reported in bottled water at concentration ranges of 4–20 ng L^{-1}.[6] Plants metabolically release Se into the atmosphere in the form of hydrogen selenide and selenates, as well as methylated Se and selenites.[1,4] As Se is chemically similar to sulfur, the sulfate transporters in the plant's roots facilitate the Se transport and distribution.[1,4,7] Atmospheric input of Se is largely influenced by natural emissions from aquatic and terrestrial environments (including volcanic eruptions) and also anthropogenic emissions from industrial processes.[4,8,9]

In the human body, Se plays an important role in regulating oxidative stress and the immune system.[1] It also acts as the catalytic center of several seleno-proteins, including glutathione peroxidase and thioredoxin reductase.[10] Deficiencies of Se in the human diet can cause thyroid dysfunction, growth retardation, and impaired bone metabolism.[11] On the other hand, selenosis (i.e., the condition of Se toxicity) can lead to pulmonary edema, garlic breath, gastrointestinal disorders, neurological damage, hair loss, and sloughing of nails.[1] Se has a relatively narrow range for optimal human consumption, with toxic levels reported at >400 μg day^{-1} and dietary deficiency at <40 μg day^{-1}.[3] It has been reported that the methylated forms of Se (e.g., DMSe) are less toxic than the inorganic Se species.[12] However, with the doses of 0.05 and 0.1 mg Se kg^{-1} of body weight, DMSe intratracheal instillation in mice has been reported to cause lung injury and inflammation.[13] Inhalation of DMSe can also result in damage to centrilobular liver cells and acute tubular injury of the kidney.[13]

The chemical fate and transport of Se in natural environments and its interactions with plants have been widely studied.[4,7] Atmospheric lifetimes of DMSe against oxidation by ozone (O_3), hydroxyl radical (OH), and nitrate radical (NO_3) have been reported, ranging from minutes to hours at typical respective oxidant concentrations.[14] However, limited details for gas-phase products of DMSe oxidation are available. Dimethyl selenoxide [$(CH_3)_2SeO$] has been identified as the major gaseous product in O_3 oxidation of DMSe, while both OH and NO_3 radical oxidations of DMSe are thought to predominantly proceed by breaking the Se–C bond, leading to the formation of formaldehyde.[15] Although not directly identified, the formation of methaneseleninic acid [CH_3Se-(O)OH] and dimethyl selenoxide as intermediates and precursors of nitrate salts is also expected from its OH and NO_3 oxidations. As a structural analogue of DMSe, dimethyl sulfide (DMS) has been reported as a major precursor leading to secondary aerosol formation in marine atmospheric environments.[16] To date, the potential of DMSe to produce inhalable secondary organic aerosol (SOA) through atmospheric oxidation has not been investigated. SOA represents a highly complex and reactive mixture of oxidized species. The dynamic nature of SOA makes the characterization of its health impacts challenging. Given the wide range of emission sources of DMSe, we hypothesized that DMSe may be a ubiquitous precursor leading to SOA formation, thereby increasing the toxicity of ambient aerosols due to the redox-active properties of Se-containing components.

In this study, we characterized the chemical properties of SOA generated from OH and O_3 oxidations of DMSe in the presence of nitric oxides (NO_x) in controlled chamber experiments and assessed the transcriptome-wide gene expression changes in human airway epithelial cells (BEAS-2B) exposed to DMSe-derived SOA. Gene expression profiling was carried out using RNA sequencing (RNA-Seq) followed by pathway enrichment analyses to identify perturbed biological pathways to provide a mechanistic understanding of DMSe-derived SOA-induced health effects.

2. MATERIALS AND METHODS

2.1. Chamber Experiments.

DMSe oxidation experiments were carried out in a ~1.3 m^3 fluorinated ethylene propylene (FEP) Teflon environmental chamber, filled with zero air (ZA). In the OH oxidation experiment, nitrous acid (HONO) vapors generated by the dropwise addition of sodium nitrite to sulfuric acid were first introduced in the chamber, followed by flowing NO to achieve ~170–300 ppbv of NO by the start of irradiation. DMSe was injected into the chamber by flowing ZA over ~1.2 μL of DMSe in a glass bulb, to achieve a mixing ratio of ~300 ppbv in the chamber. After allowing the content of the bag to mix for 10 min, black lights (peak radiation intensity at ~350 nm) surrounding the chamber were turned on to initiate photooxidation. Based on previous characterization experiments of octane oxidation, the expected OH concentration in the chamber is at least 3×10^7 molecules cm^{-3}.[17] In the O_3 oxidation experiment, O_3 was first introduced in the chamber by flowing ZA through a λ = 185 nm lamp source (UVP Ltd.). After reaching ~250 ppbv of O_3 in the chamber, O_3 injection was stopped, and vapors of DMSe (1.2 μL) were injected into the bag. Once O_3 mixing ratio decreased to 50 ppbv, additional O_3 was injected to the bag in a similar manner to maintain a mixing ration of ~50–150 ppbv. During the O_3 oxidation experiment, background NO_x in the chamber before the reaction was less than 2 ppbv. Relative humidity in the chamber was low (<25%) in both experiments. A summary of the experimental conditions is provided in Table S1.

During the experiments, gas-phase mixing ratios of O_3 and NO_x were monitored by a UV photometric ozone analyzer (Thermo, model 49i) and a chemiluminescence analyzer (Thermo, model 42i), respectively. Aerosol size distributions were measured by a scanning electrical mobility spectrometer (SEMS, Brechtel Manufacturing Inc.), while aerosol composition was measured by a mini aerosol mass spectrometer (mAMS) with a compact time-of-flight mass spectrometer detector (Aerodyne Research, Inc.). DMSe-derived SOA mass concentrations were determined by standard analysis of the unit-mass resolution spectra of mAMS (using SQUIRREL ToF-AMS Analysis Toolkit, version 1.61), as well as size distribution measurements by SEMS.[18,19] DMSe-derived SOA densities used in SEMS mass calculations were determined by comparing vacuum aerodynamic-based mass distributions from the mAMS with mobility-based volume distributions of the SEMS.[20] Given the performance of mAMS during the experiments (mass spectrometer resolution of ~1100 and mass accuracy of better than 1.2 ppm at m/z 40 and better than 3 ppm at m/z 184), multipeak fitting routines written for high-resolution analysis of mAMS spectra were applied to $m/z < 113$ amu (using PIKA ToF-AMS Analysis Toolkit, version 1.21) to gain more detailed insights into the composition of DMSe-derived SOA.[21] It is worth noting that >97% of the detected aerosol mass in both experiments was at $m/z < 113$ amu. The high-resolution ion list of PIKA was adjusted to include Se-containing fragments (and their corresponding isotopic fragments) in the fitting routine.

2.2. Aerosol Sample Collection and Extraction.

At the end of each experiment, DMSe-derived SOA samples were collected onto 47 mm Teflon membrane filters and stored at −20 °C for 2 weeks until extraction. Filters were

extracted with 23 mL of high-purity methanol [high-performance liquid chromatography (HPLC) grade, Fisher Scientific], followed by 50 min of sonication. After sonication, the extracted solution was transferred to a clean vial, and the methanol solvent was dried off under a gentle stream of nitrogen gas. Then, the extracted DMSe-derived SOA constituents were stored at −20 °C (typically for a day) until further analysis.

2.3. Dithiothreitol (DTT) Assay.

DTT assays were conducted to measure the oxidative potential (i.e., thiol reactivity) of DMSe-derived SOA products from both O_3 and OH oxidation experiments. The DTT assay procedures were carried out based on those published by Kramer et al.[22] Briefly, an aqueous buffer solution was made with potassium phosphate monobasic/sodium hydroxide (0.05 M, pH 7.4) and 1 mM ethylenediaminetetraacetic acid (EDTA). The reaction mixtures ($n = 3$) containing 1 μg of DMSe-derived SOA extracts and 2.5 nmol of DTT were incubated at 37 °C for 30 min; then, the remaining DTT was quenched with 10 nmol of 5,5′-dithiobis-(2-nitrobenzoic acid) (DTNB) to make the final volume of 135 μL. The reaction between DTNB and DTT produced 5-thio-2-nitrobenzoic acid (TNB) that can be measured by its absorbance at 412 nm using a UV–vis spectrophotometer (Beckman DU-640). The DTT consumption rate (expressed as nmol DTT consumed per min per μg of sample) was quantified in comparison with blank filter samples. To examine the potential for sample degradation during storage, filter samples from O_3 and OH oxidation experiments were also analyzed immediately after collection.

2.4. Cell Culture and Exposure.

BEAS-2B cells, obtained from the American Type Culture Collection (ATCC), were originally derived from the normal bronchial epithelium of a healthy individual. Cells were transformed by infection with a replication-defective SV40/adenovirus 12 hybrid and cloned to create an immortalized cell line.[23] Cells were cultured in commercially purchased Gibco LHC-9 medium (1×) (Invitrogen) and grown at 37 °C and 5% CO_2 in a humidified incubator. Cells were seeded in 24-well plates at a density of 2.5×10^4 cells per well in 250 μL of LHC-9 medium for 2 days prior to exposure. At the time of exposure, cells reached a 60–70% confluence. Dried DMSe-derived SOA extracts were reconstituted with the LHC-9 medium. Cells were washed with phosphate-buffered saline (PBS) and then exposed to DMSe-derived SOA extracts from the O_3 and OH oxidation experiments at the concentration of 10 μg mL^{-1} for 24 h. Cells exposed to extracts of blank filters were included as negative controls.

2.5. RNA Isolation and Sequencing.

After 24 h of exposure, cells were lysed with 350 μL of TRI reagent (Zymo Research) for total RNA isolation. Isolated RNA samples were further purified using the spin column-based Direct-zol RNA MiniPrep kit (Zymo Research). Extracted RNA samples were stored at −80 °C until processing. Nanodrop ND-1000 spectrophotometer (Thermo Fisher Scientific, Wilmington, DE) and Agilent 2100 Bioanalyzer (Agilent, Santa Clara, CA) were used to measure the RNA quality and concentrations. The 260/280 nm absorbance ratios of all samples were determined to be >1.8. The RNA integrity number (RIN) scores from Bioanalyzer were >7. Following the manufacturer's recommendations, RNA-Seq libraries

were prepared using the NEBNext ultra II Directional RNA Library Prep Kit for Illumina NextSeq. 500 high output 75bp single end analysis. RNA-Seq was performed at the University of California, Riverside-Institute for Integrative Genome Biology (IIGB). The read data were deposited in the sequence read archive (SRA) BioSample database (SRA accession number: PRJNA539990).

2.6. RNA-Seq Data Analysis.

After sequencing, FastQC (version 0.11.7)[24] was used for read quality assessment. Trimming was obtained using Trimmomatic (version 0.35).[25] Bases before positions 13 and after 72 were cropped with CROP:72 and HEADCROP:13 parameters. Reads that are at least 50 bases long were kept using MINLEN:50. Then, raw reads were aligned to the human genome version hg19 with HISAT2 (version 2.1.0).[26] The aligned files were converted to bam files, sorted, and indexed with samtools (version 1.9).[27] Subread (version 1.6.2) tool was used for counting reads of the UCSC Genome Browser annotated coding sequence (CDS) using the featureCounts commands.[28] Normalization and differential gene expression analysis were carried out using three different packages, including DESeq. 2 (version 1.18.1), edgeR (version 3.20.9), and Limma package (version 3.34.9) in R (version 3.4.4).[29–31] The combination of multiple data processing tools that use different models and normalization methods to identify differentially expressed genes (DEGs) improves the sensitivity of DEG identification and provides more reliable and robust results than the individual solutions.[32,33]

Cutoffs used for DEGs between treated and untreated samples were identified and considered significant if the p value was ≤0.01, false discovery rate (FDR) value was ≤0.01, and the absolute Log_2 fold change (Log_2 FC) was ≥1. The workflow for RNA-Seq data analysis is provided in Figure S1. The Log_2 FC values of selected genes are provided in Figures S2 and S3.

2.7. Pathway Enrichment Analysis.

For significantly altered genes, pathway enrichment analyses were performed to identify perturbed biological pathways from target gene sets using the ConsensusPathDB database.[34] To interpret the function of altered genes, over-representation analyses were carried out. Based on the hypergeometric distribution, the significance level of observed overlap between the members of predefined pathways and the input DEGs was calculated. Criteria of (1) a minimum overlap of two genes between the input list and pathways, and (2) a p value cutoff of 0.01 were set.[35] ClueGO (a Cytoscape app, version 2.5.4) was used for visualization of enriched pathways.[36]

3. RESULTS

3.1. Aerosol Production and Composition.

Both OH and O_3 oxidation experiments resulted in DMSe-derived SOA formation. Despite the intense nucleation during the O_3 experiments (e.g., Figure 1a), the total mass of DMSe-derived SOA formed from the O_3 oxidation (10–20 $\mu g\ m^{-3}$) was significantly lower than in

the OH experiments (250–300 $\mu g\ m^{-3}$) at similar oxidation times and with similar amounts of DMSe injected (e.g., Figure 1b).

Although the chamber concentration of DMSe was not monitored during the experiments, given the differences in DMSe oxidation rate constants with OH (6.8×10^{-11} cm^3 $molecule^{-1}$ s^{-1})[14] and O_3 (6.8×10^{-17} cm^3 $molecule^{-1}$ s^{-1})[14] and representative oxidant concentrations during the experiments ($[OH]_{average} = 3 \times 10^7$ molecule cm^{-3} and $[O_3]_{average}$ = 75–100 ppbv), we expect to have reacted only ~50–60% (~160–180 ppbv) of DMSe with O_3 after 80–100 min (assuming the secondary production of OH was negligible), while a negligible fraction should have remained during the same time in the OH oxidation experiment. Further discussion on DMSe's potential to form SOA is provided in Section 4.1. As shown in Figure 1b, in both experiments, estimated mass concentrations using mAMS unit-mass resolution spectra, along with the standard relative ionization efficiency of organics ($RIE_{org} = 1.4$) and unity collection efficiency, agreed well with the total mass concentrations estimated from the measured size distributions and inferred SOA densities.

High-resolution analysis of mAMS spectra with the modified HR-ion list suggests that on average ~52–54% of the observed mass concentration in the range of $m/z < 113$ was from fragments containing Se, while ~18–22% of the mass stemmed from organic fragments lacking Se in their structures (Figure 2a). The contribution of the Se-containing ions was similar between the O_3 and OH oxidation experiments (Figure 2b), suggesting that the composition of DMSe-derived SOA is relatively similar for both pathways.

In both experiments, ~20–25% of aerosol mass was from nitrate (Figure 2a); however, given the different NO^+/NO_2^+ ratios, different compounds likely contribute to the nitrate concentrations in the OH and O_3 oxidation experiments (Figure S4). During the first ~40 min after the start of the reaction, there is evidence for the formation of organonitrates in both systems, given the higher ratio of NO^+/NO_2^+ relative to that of ammonium nitrate. However, during the OH experiment, the ratio decreased to values lower than that of ammonium nitrate after ~60 min, while in the O_3 experiment, the ratio approached ammonium nitrate calibrations (Figure S4). These observations suggest the formation of nitrated salts or nitro-organics in the OH experiment and the formation of nitric acid in the O_3 experiment.

3.2. Aerosol Oxidative Potential.

The oxidative potential of aerosol is expressed as DTT consumption rate normalized to the particulate matter (PM) mass (pmol min^{-1} μg^{-1}). Both aerosol samples collected from OH and O_3 oxidation experiments have similar DTT consumption rates of ~77 pmol min^{-1} μg^{-1}, suggesting the presence of common oxidizing moieties in both aerosol systems. Note that the reactive components in DMSe-derived SOA did not seem to decay rapidly under the given storage duration and conditions as evidenced in the similarity of DTT activity between stored and freshly analyzed filter samples (Figure S5). The DTT assay has been widely used as an indicator for total particle-bound oxidants in aerosol constituents.[37] In comparison with other sources of PM, DMSe-derived SOA have DTT consumption rates higher than ambient PM (10–70 pmol min^{-1} μg^{-1}),[38] SOA from isoprene, toluene, and α-pinene (2.1–57.5 pmol min^{-1} μg^{-1}),[22,39,40] and diesel exhaust particles (1–61 pmol min^{-1} μg^{-1}).[41] The

DTT consumption rates of DMSe-derived SOA are comparable to cooking OA (90 ± 51 pmol min^{-1} per PM), but less than biomass burning OA (151 ± 20 pmol min^{-1} μg^{-1})[38] and naphthalene SOA (153.4 ± 49.2 pmol min^{-1} μg^{-1}) that potentially constitute redox-active quinones.[38]

3.3. Differential Gene Expression from RNA-Seq Data.

RNA-Seq was performed to detect differential gene expression in BEAS-2B cells exposed to DMSe-derived SOA (from both OH and O_3 oxidation experiments) versus the control groups that were exposed to the blank filter extracts. The lactate dehydrogenase (LDH) assay analysis of the cellular samples indicated no significant cell death after 24 h of exposure; therefore, RNA-seq results represent the true transcriptional change of the live cells (Figure S6). From RNA-Seq quality analysis, the quality metrics indicated base composition bias before 13 and after 72 bp positions, which could be due to the unbalanced selection of random primers. Therefore, those base positions were cropped prior to alignment. On average, we obtained 24.8 million mapped reads, with a mapping rate of 90.81% (Table S2). From 23 393 UCSC annotated human CDS, we retained ~55% of genes for subsequent analyses with transcriptional signal fragments per million (fpm) ≥1 in DESeq. 2. This percentage was the same when using counts per million (cpm) ≥1 as a threshold in edgeR and limma.

With the sorting criteria of Log_2 FC |±1|, p value = 0.01, false discovery rate (FDR)-adjusted p value = 0.01, DESeq. 2, edgeR, and Limma resulted in 2619 and 2616, 2605 and 2687, and 1229 and 1258 DEGs for O_3 and OH, respectively. The three sets of DEGs obtained from DESeq. 2, edgeR, and limma were intersected to identify common DEGs. As shown in the intersections of Venn diagrams in Figure 3, we identified 1196 common DEGs from exposure to O_3 oxidation products (862 upregulated and 334 downregulated) and 1232 common DEGs from exposure to OH oxidation products (875 upregulated and 357 downregulated) for the downstream pathway enrichment analysis.

3.4. Perturbed Biological Pathways.

Significantly altered biological pathways were identified using the Consensus-PathDB database (Tables S3 and S4). The input of DEGs was categorized into six groups based on up- and downregulation of genes: (1) upregulated by both O_3 and OH oxidation products, (2) upregulated by O_3 only, (3) upregulated by OH only, (4) downregulated by both O_3 and OH oxidation products, (5) downregulated by O_3 only, and (6) downregulated by OH only (Figure S7). Figure 4 shows the major biological pathways enriched for upregulated and downregulated DEGs by both O_3 and OH oxidation products.

Top pathways that are enriched by upregulated common DEGs from both O_3 and OH oxidation products include genotoxicity, p53 signaling, and mitogen-activated protein kinase (MAPK) signaling (Table S3). On the other hand, downregulated common DEGs by both O_3 and OH oxidation products enriched pathways mostly associated with the metabolic regulation of glucose, as well as the interleukins IL-4 and IL-13 signaling that are related to the pathogenesis of allergic airway disorders (Table S4).

4. DISCUSSION

4.1. DMSe-Derived SOA Yields.

Both OH and O_3 oxidations of DMSe resulted in the formation and growth of DMSe-derived SOA. Considering the estimated amounts of reacted DMSe in each experiment, our results suggest DMSe-derived SOA formation yields of ~23 and ~2% in the OH and O_3 oxidation experiments, respectively (Table S1). The significantly lower yields in O_3 oxidation experiments suggest the formation of relatively more volatile products under these conditions. These SOA formation yields are in the same range as the yields observed in a nonseeded chamber or flow tube photooxidation experiments of other naturally emitted hydro-carbons, such as isoprene and α-pinene.[42–44] Further discussion on the potential abundance of atmospheric DMSe oxidation products is presented in Section 4.7. Note that these SOA yields are likely underestimated since vapor and particle losses to the chamber walls were not corrected for, and the observed nitrate components were not considered as DMSe-derived SOA. Despite the much lower formation yield in the O_3 oxidation experiment, bulk DMSe-derived SOA composition was very similar to that in the OH oxidation experiment, which could potentially explain similar values of aerosol oxidative potential measured for DMSe-derived SOA in the two systems.

4.2. PM Oxidative Potential and DMSe-Derived SOA-Induced Oxidative Damage.

High PM oxidative potential measured by the DTT assay has been associated with the ability of PM to generate reactive oxygen species (ROS).[45] Previously, the DTT activities of ambient PM have been largely attributed to the presence of transition metals and quinones.[46] In this study, the oxidative potential of DMSe-derived SOA was assessed and found to contribute to high DTT consumption rates, which supports our hypothesis that DMSe-derived SOA possesses redox-active properties. Recent studies have also indicated that PM oxidative potential can be directly linked to the reactivity of PM constituents toward thiol functional groups within biomolecules leading to cellular oxidative stress.[47,48] Cellular oxidative stress can be attributed to an imbalance between ROS production (from both exogenous and endogenous sources) and their elimination through protective mechanisms by antioxidants. Disbalance in these pathways is the leading cause of a variety of injuries, including acute and chronic inflammations, genome instability and mutation, pulmonary fibrosis, obesity, diabetes, and atherosclerosis.[49] Prior studies have established that through metabolic processes, Se compounds have the potential to induce genotoxicity via the generation of ROS.[50] Relative expression of oxidative stress and antioxidant-related genes are consistent with DTT results (Figure S2). With exposure to DMSe-derived SOA in BEAS-2B cells, several pathways associated with oxidative damage, genotoxicity, glutathione metabolism, biological oxidation, and DNA damage response were perturbed and are discussed in the next sections. Results from both DTT assays and pathway enrichment analysis suggest that Se-containing moieties in DMSe-derived SOA might be important in ROS-induced oxidative damage.

4.3. DNA Damage, Genotoxicity, and Activation of p53-Mediated Stress Response.

The upregulated DEGs from both O_3 and OH oxidation experiments revealed the activation of p53 signaling pathway in response to DMSe-derived SOA exposure in BEAS-2B cells

(Table S3 and Figure 4a). Tumor suppressor protein p53 is encoded by the *TP53* gene, which is one of the most commonly mutated genes in human cancer,[51] including lung cancer.[52] More than half of all tumors exhibit mutations in either *TP53* or MDM2 protooncogene (*MDM2*) genes, whose protein products control p53 activity.[51,53] The affinity of p53 for MDM2 is reduced when ataxia-telangiectasia mutated (ATM) protein kinase (Table S3, FDR = 7.22×10^{-2}) phosphorylates p53, which consequently results in reduced p53 degradation by MDM2 and thus enhances p53 protein stability and activity.[54] The functions of p53 are complex; under normal conditions, p53 expression is very low inside the cell, but it is activated in response to oxidative, genotoxic, or oncogenic stress; p53 exerts its activities as tumor-suppressive, pro-oxidant, and antioxidant.[51,55] Under mild stress, activated p53 acts as a prooxidant and mediates the activation of tumor protein 53-induced nuclear protein 1 (*TP53INP1*) and cyclin-dependent kinase inhibitor 1A (*CDKN1A*) to induce cell cycle arrest in G1 to allow cells to repair and recover from damage. Under prolonged stress or rapid DNA damage, p53 acts as an antioxidant and activates the BCL2 binding component 3 (*BBC3*) and phorbol-12-myristate-13-acetate-induced protein 1 (*PMAIP1*) genes that produce proapoptotic proteins to neutralize the DNA damage.[51,55] In addition, p53 can also act as an upstream activator to regulate mitogen-activated protein kinase (MAPK) signaling in response to DNA damage from external insults.[56] Overall, DMSe-derived SOA can activate p53 through the genotoxicity pathway, which could potentially result in various adverse cellular events like DNA damage, heat shock, hypoxia, and oncogene overexpression.[57]

4.4. Dysregulation of Metabolic Pathways with p53 Activation.

The downregulated DEGs identified from this study revealed the dysregulation of metabolic pathways associated with cholesterol biosynthesis, glycolysis, gluconeo-genesis, and fatty acid synthesis (Table S4 and Figure 4b).[58] Upon the activation of p53 under stress, many cellular processes that control energy and metabolism are negatively regulated to maintain homeostasis. Recent studies have shown the connection between p53, energy metabolism, and metabolic diseases, including type II diabetes mellitus.[51,55] Moreover, p53 can also indirectly control glycolysis by regulating the phosphatidylinositol 3-kinase/protein kinase b (PI3K/Akt) pathways (Table S4, FDR = 4.70×10^{-5}). Specifically, the PI3K/Akt pathway can be negatively regulated by the p53 target genes, including the tumor suppressor gene phosphatase and tensin homologue deleted on chromosome 10 (*PTEN*) that is frequently inactivated by mutation.[51] As the PTEN phosphatase activity is the major antagonist of Akt, PTEN could affect the p53 protein levels and stability by keeping Akt inactive,[55,59] and thus PTEN would be an essential component of the p53 response upon DNA damage. At the same time, p53 is linked to enhancing the transcription of *PTEN*.[60] However, under reduced nutrient or energy levels, the Akt and adenosine 5′-monophosphate (AMP)-activated protein kinase (AMPK) (Table S3, FDR = 1.88×10^{-3}) fail to be activated, which can subsequently induce p53. As a result, it is clear that p53 plays a pivotal role in metabolic regulation.[55] Through suppression of the peroxisome proliferator-activated receptor-γ coactivator-1α (PGC-1α), p53 also influences the insulin resistance that is critical in the development of type II diabetes and prediabetes.[51,61] Notably, the Warburg effect (FDR = 1.33×10^{-3}) was also found to be significantly enriched in the current study (Table S3). The Warburg effect describes the increased usage of glycolysis for adenosine 5′-triphosphate (ATP) synthesis

rather than using oxidative phosphorylation, which is a metabolic hallmark of cancer cells that rewire their metabolism to promote growth and survival.[55] It has been suggested that the Warburg effect may provide unifying insights into the progression of cancer and type II diabetes mellitus.[62] Overall, the perturbed biological pathways identified in this study (Tables S3 and S4) are coherent and conclusively support the potential significance of p53-mediated metabolic dysregulation caused by DMSe-derived SOA exposure.

4.5. Signaling Associated with Allergic Airway Inflammation.

Downregulated IL-4/IL-13 signaling (FDR = 6.40×10^{-4}) and neutrophil degranulation (FDR = 1.61×10^{-2}) pathways were both observed in this study (Table S4), consistent with the previous reports that IL-4 and IL-13 can suppress excessive neutrophil accumulation.[63] Although neutrophils were directly not tested in the current study, genes involved in neutrophil degranulation were found differentially expressed in BEAS-2B. Among these DEGs, mutation in *SERPINA1* has been linked to low levels of α−1-antitrypsin (AAT) in alveolar epithelial cells that may lead to premature development of pulmonary emphysema.[64] Notably, perturbations in various inflammatory responses and signaling pathways revealed the potential interplay between oxidative damage and inflammation upon DMSe-derived SOA exposure, which may result in the production of soluble mediators to activate the signal transducer and activator of transcription 3 (STAT3) and MAPK that mediate the expression of a variety of genes in response to cellular stimuli.[49,65] Chronic inflammation can contribute to tumor development through the induction of oncogenic mutations, genomic instability, early tumor promotion, and enhanced angiogenesis. In type 2 inflammatory responses associated with the pathogenesis of asthma and allergies, IL-4 and IL-13 are the signature cytokines that can be triggered by allergens;[66] however, IL-4 and IL-13 play distinct roles in allergic inflammatory states. Briefly, IL-4 regulates Th2 cell proliferation and survival that has been shown to be essential in the initiation of allergic airway responses, while IL-13 contributes to the pathological features of diseases (e.g., mucus production, airway smooth muscle alterations, and subepithelial fibrosis).[67] Recent studies have shown that the activation of IL-4/IL-13−STAT6 and ROS-epidermal growth factor receptor (EGFR) signaling pathways is associated with airway mucin overproduction induced by foreign stimuli,[68] as well as enhanced epithelial repair in response to lung injury.[69] Together with the significant ROS generation potential (as measured by DTT) and the identified EGFR signaling pathway, our findings highlight the potential significance of DMSe-derived SOA in modulating allergic airway inflammation.

4.6. Potential Limitations.

When interpreting the results of the current study, some potential limitations should be considered. First, the oxidative potential of DMSe-SOA was measured using an acellular DTT assay to approximate the ability of PM to generate ROS or reactivity toward thiols. Recent studies have indicated that DTT activity can only represent part of PM-bound ROS.[70] Measurement of ROS within cells will provide more direct evidence to determine the cellular oxidative stress conditions and warrants future work. Also, the initial concentration of DTT used in the assay has been reported to influence the DTT consumption rates.[71] Caution should be taken when intercomparing the DTT assay results from different studies. In addition, owing to the nature of the hard ionization technique used by mAMS, the

composition of the highly fragmented DMSe-derived SOA products was obtained. To identify specific moieties or functional groups of DMSe-derived SOA contributing to ROS generation, comprehensive analysis that can retain molecular information is necessary. DMSe-derived SOA samples were extracted with methanol, which may have selectively enriched certain types of DMSe-derived SOA constituents. Furthermore, the use of an immortalized cell line (BEAS-2B) may not faithfully represent the untransformed human airway epithelium, but it provides reproducible results critical to gaining initial insights into the cellular response to DMSe-derived SOA exposure. Finally, as RNA-Seq and pathway enrichment analysis have enabled the rapid identification of pathway perturbations at the transcriptional level, functional validation will be required to demonstrate the effects on the changes of phenotypes.

4.7. Atmospheric Implications.

Selenium contamination is associated with a broad spectrum of natural and anthropogenic activities, but the sources and sinks are not well constrained in the atmosphere. Concentrations of Se measured in ambient aerosols have been reported to range from ~1.5 to 30 ng m^{-3}.[72] A wide range of selenium volatilization rates from terrestrial emissions in California have also been reported (~20 μg Se m^{-2} day^{-1} for bare soil and up to 430 μg Se m^{-2} day^{-1} in biotreated soil).[73,74] Moreover, Karlson et al. reported that DMSe emissions potentially can increase with the onset of the warmer temperatures, during the summer season.[75] In San Joaquin Valley, DMSe contributes to 90% of volatile Se.[76] Assuming a 1 acre source area, the emission rates mentioned above translate to ~4–80 pptv day^{-1} emissions of DMSe in a 1.5 km deep planetary boundary layer. Considering typical, nonpolluted daytime OH and nighttime O_3 concentrations (4×10^6 molecule cm^{-3} and 50 ppbv, respectively) with the estimates of our DMSe-derived SOA formation yield, at least ~0.2–80 ng m^{-3} of DMSe-derived SOA can be produced in 4 h during day or night. Although Se-rich soils might not be in close proximity to populated areas, since fine particles have lifetimes of ~7–10 days, once formed in at the atmosphere, DMSe-derived SOA particles could potentially be transported away and pose health risks in areas downwind of high DMSe emission regions. Furthermore, if agricultural fields contain high Se in the soil, field workers could potentially be in direct exposure to significant amounts of DMSe-derived SOA, especially during the warmer months.

Overall, the atmospheric oxidation of DMSe produces SOA with high oxidative potential. Transcriptomic gene expression profiling followed by pathway enrichment analysis revealed that major biological pathways perturbed by DMSe-derived SOA are associated with elevated genotoxicity, DNA damage, and p53-mediated stress responses, as well as dysregulated metabolic activities and cytokine signaling that plays crucial roles in allergic airway inflammation. Future work is required to examine atmospheric emissions of DMSe and gain a more detailed molecular composition of DMSe-derived SOA. To fully assess the environmental health impacts of DMSe-derived SOA, direct measures of ROS production and validation of the perturbed biological functions in primary airway epithelial cells and other cell types would also be valuable.

Supplementary Material

Refer to Web version on PubMed Central for supplementary material.

ACKNOWLEDGMENTS

The authors gratefully acknowledge support from USDA-NIFA Hatch (accession no. 1015963, project no. CA-R-ENS-5072-H) and assistance from Donna Sueper (Aerodyne Research Inc.) for the high-resolution selenium analysis of the mAMS spectra. The authors also thank Alexa Canchola for her experimental assistance.

REFERENCES

(1). Gupta M; Gupta S An overview of selenium uptake, metabolism, and toxicity in plants. Front. Plant. Sci 2017, 7, No. 2074. [PubMed: 28123395]

(2). Mehdi Y; Hornick J-L; Istasse L; Dufrasne I Selenium in the environment, metabolism and involvement in body functions. Molecules 2013, 18, 3292. [PubMed: 23486107]

(3). Winkel LHE; Johnson CA; Lenz M; Grundl T; Leupin OX; Amini M; Charlet L Environmental selenium research: from microscopic processes to global understanding. Environ. Sci. Technol 2012, 46, 571–579. [PubMed: 22129299]

(4). Ullah H; Liu G; Yousaf B; Ali MU; Irshad S; Abbas Q; Ahmad R A comprehensive review on environmental transformation of selenium: recent advances and research perspectives. Environ. Geochem. Health 2019, 41, 1003–1036. [PubMed: 30267320]

(5). Wen H; Carignan J Reviews on atmospheric selenium: emissions, speciation and fate. Atmos. Environ 2007, 41, 7151–7165.

(6). Guadayol M; Cortina M; Guadayol JM; Caixach J Determination of dimethyl selenide and dimethyl sulphide compounds causing off-flavours in bottled mineral waters. Water Res 2016, 92, 149–155. [PubMed: 26852288]

(7). Wadgaonkar SL; Nancharaiah YV; Esposito G; Lens PN Environmental impact and bioremediation of seleniferous soils and sediments. Crit. Rev. Biotechnol 2018, 38, 941–956. [PubMed: 29302994]

(8). Frie AL; Dingle JH; Ying SC; Bahreini R The effect of a receding saline lake (the Salton Sea) on airborne particulate matter composition. Environ. Sci. Technol 2017, 51, 8283–8292. [PubMed: 28697595]

(9). Blazina T; Läderach A; Jones GD; Sodemann H; Wernli H; Kirchner JW; Winkel LH Marine primary productivity as a potential indirect source of selenium and other trace elements in atmospheric deposition. Environ. Sci. Technol 2017, 51, 108–118. [PubMed: 27959548]

(10). Kaur N; Sharma S; Kaur S; Nayyar H Selenium in agriculture: a nutrient or contaminant for crops? Arch. Agron. Soil Sci 2014, 60, 1593–1624.

(11). Reeves M; Hoffmann P The human selenoproteome: Recent insights into functions and regulation. Cell. Mol. Life Sci 2009, 66, 2457–2478. [PubMed: 19399585]

(12). Karlson U; Frankenberger WT Volatilization of selenium from agricultural evaporation pond sediments. Sci. Total Environ 1990, 92, 41–54. [PubMed: 2326625]

(13). Cherdwongcharoensuk D; Henrique R; Upatham S; Pereira AS;Águas AP Tubular kidney damage and centrilobular liver injury after intratracheal instillation of dimethyl selenide. Toxicol. Pathol 2005, 33, 225–229. [PubMed: 15902965]

(14). Atkinson R; Aschmann SM; Hasegawa D; Thompson-Eagle ET; Frankenberger WT Kinetics of the atmospherically important reactions of dimehtyl selenide. Environ. Sci. Technol 1990, 24, 1326–1332.

(15). Rael RM; Tuzaon EC; Frankenberger WT Gas-phase reactions of dimethyl selenide with ozone and the hydroxyl and nitrate radicals. Atmos. Environ 1996, 30, 1221–1232.

(16). Barnes I; Hjorth J; Mihalopoulos N Dimethyl sulfide and dimethyl sulfoxide and their oxidation in the atmosphere. Chem. Rev 2006, 106, 940–975. [PubMed: 16522014]

(17). Dingle JH; Zimmerman S; Frie AL; Min J; Jung H; Bahreini R Complex refractive index, single scattering albedo, and mass absorption coefficient of secondary organic aerosols generated from oxidation of biogenic and anthropogenic precursors. Aerosol Sci. Technol 2019, 53, 449–463.

(18). Canagaratna MR; Jayne JT; Jimenez JL; Allan JD; Alfarra MR; Zhang Q; Onasch TB; Drewnick F; Coe H; Middlebrook AM; Delia A; Williams LR; Trimborn AM; Northway MJ; DeCarlo PF; Kolb CE; Davidovits P; Worsnop DR Chemical and microphysical characterization of ambient aerosols with the aerodyne aerosol mass spectrometer. Mass Spectrom. Rev 2007, 26, 185–222. [PubMed: 17230437]

(19). Bahreini R; Keywood MD; Ng NL; Varutbangkul V; Gao S; Flagan RC; Seinfeld JH; Worsnop DR; Jimenez JL Measurements of secondary organic aerosol from oxidation of cycloalkenes, terpenes, and m-xylene using an Aerodyne aerosol mass spectrometer. Environ. Sci. Technol 2005, 39, 5674–5688. [PubMed: 16124302]

(20). DeCarlo PF; Slowik JG; Worsnop DR; Davidovits P; Jimenez JL Particle morphology and density characterization by combined mobility and aerodynamic measurements. part 1: theory. Aerosol Sci. Technol 2004, 38, 1185–1205.

(21). Bahreini R; Middlebrook AM; Brock CA; de Gouw JA; McKeen SA; Williams LR; Daumit KE; Lambe AT; Massoli P; Canagaratna MR; Ahmadov R; Carrasquillo AJ; Cross ES; Ervens B; Holloway JS; Hunter JF; Onasch TB; Pollack IB; Roberts JM; Ryerson TB; Warneke C; Davidovits P; Worsnop DR; Kroll JH Mass spectral analysis of organic aerosol formed downwind of the deepwater horizon oil spill: field studies and laboratory confirmations. Environ. Sci. Technol 2012, 46, 8025–8034. [PubMed: 22788666]

(22). Kramer A; Rattanavaraha W; Zhang Z; Gold A; Surratt J; Lin Y Assessing the oxidative potential of isoprene-derived epoxides and secondary organic aerosol. Atmos. Environ 2016, 130, 211–218.

(23). Reddel RR; Ke Y; Gerwin BI; McMenamin MG; Lechner JF; Su RT; Brash DE; Park J-B; Rhim JS; Harris CC Transformation of human bronchial epithelial cells by infection with SV40 or adenovirus-12 SV40 hybrid virus, or transfection via strontium phosphate coprecipitation with a plasmid containing SV40 early region genes. Cancer Res 1988, 48, 1904–1909. [PubMed: 2450641]

(24). Andrews S A quality control tool for high throughput sequence data. FastQC, 2014 http://www.bioinformatics.babraham.ac.uk/projects/fastqc/.

(25). Bolger AM; Lohse M; Usadel BJB Trimmomatic: a flexible trimmer for Illumina sequence data. Bioinformatics 2014, 30, 2114–2120. [PubMed: 24695404]

(26). Kim D; Langmead B; Salzberg SL HISAT: a fast spliced aligner with low memory requirements. Nat. Methods 2015, 12, 357–360. [PubMed: 25751142]

(27). Li H; Handsaker B; Wysoker A; Fennell T; Ruan J; Homer N; Marth G; Abecasis G; Durbin R The sequence alignment/map format and SAMtools. Bioinformatics 2009, 25, 2078–2079. [PubMed: 19505943]

(28). Liao Y; Smyth GK; Shi W The Subread aligner: fast, accurate and scalable read mapping by seed-and-vote. Nucleic Acids Res 2013, 41, e108. [PubMed: 23558742]

(29). Love MI; Huber W; Anders S Moderated estimation of fold change and dispersion for RNA-seq data with DESeq. 2. Genome Biol 2014, 15, No. 550. [PubMed: 25516281]

(30). Ritchie ME; Phipson B; Wu D; Hu Y; Law CW; Shi W; Smyth GK Limma powers differential expression analyses for RNA-sequencing and microarray studies. Nucleic Acids Res 2015, 43, e47. [PubMed: 25605792]

(31). Robinson MD; McCarthy DJ; Smyth GK edgeR: a Bioconductor package for differential expression analysis of digital gene expression data. Bioinformatics 2010, 26, 139–140. [PubMed: 19910308]

(32). Costa-Silva J; Domingues D; Lopes FM RNA-Seq differential expression analysis: An extended review and a software tool. PLoS One 2017, 12, No. e0190152. [PubMed: 29267363]

(33). Assefa AT; De Paepe K; Everaert C; Mestdagh P; Thas O; Vandesompele J Differential gene expression analysis tools exhibit substandard performance for long non-coding RNA-sequencing data. Genome Biol 2018, 19, No. 96. [PubMed: 30041657]

(34). Kamburov A; Wierling C; Lehrach H; Herwig R ConsensusPathDB–a database for integrating human functional interaction networks. Nucleic Acids Res 2009, 37, D623–D628. [PubMed: 18940869]

(35). Zhavoronkov A; Buzdin AA; Garazha AV; Borisov NM; Moskalev AA Signaling pathway cloud regulation for in silico screening and ranking of the potential geroprotective drugs. Front. Genet 2014, 5, No. 49. [PubMed: 24624136]

(36). Bindea G; Mlecnik B; Hackl H; Charoentong P; Tosolini M; Kirilovsky A; Fridman W-H; Pages F; Trajanoski Z; Galon J ClueGO: a Cytoscape plug-in to decipher functionally grouped gene ontology and pathway annotation networks. Bioinformatics 2009, 25, 1091–1093. [PubMed: 19237447]

(37). Cho AK; Sioutas C; Miguel AH; Kumagai Y; Schmitz DA; Singh M; Eiguren-Fernandez A; Froines JR Redox activity of airborne particulate matter at different sites in the los angeles basin. Environ. Res 2005, 99, 40–47. [PubMed: 16053926]

(38). Verma V; Fang T; Xu L; Peltier RE; Russell AG; Ng NL; Weber RJ Organic aerosols associated with the generation of reactive oxygen species (ROS) by water-soluble PM2.5. Environ. Sci. Technol 2015, 49, 4646–4656. [PubMed: 25748105]

(39). Jiang H; Jang M; Sabo-Attwood T; Robinson SE Oxidative potential of secondary organic aerosols produced from photooxidation of different hydrocarbons using outdoor chamber under ambient sunlight. Atmos. Environ 2016, 131, 382–389.

(40). Tuet WY; Chen Y; Xu L; Fok S; Gao D; Weber RJ; Ng NL Chemical oxidative potential of secondary organic aerosol (SOA) generated from the photooxidation of biogenic and anthropogenic volatile organic compounds. Atmos. Chem. Phys 2017, 17, 839–853.

(41). Cheung KL; Polidori A; Ntziachristos L; Tzamkiozis T; Samaras Z; Cassee FR; Gerlofs M; Sioutas C Chemical characteristics and oxidative potential of particulate matter emissions from gasoline, diesel, and biodiesel cars. Environ. Sci. Technol 2009, 43, 6334–6340. [PubMed: 19746734]

(42). Kroll JH; Ng NL; Murphy SM; Flagan RC; Seinfeld JH Secondary organic aerosol formation from isoprene photooxidation. Environ. Sci. Technol 2006, 40, 1869–1877. [PubMed: 16570610]

(43). Lambe AT; Chhabra PS; Onasch TB; Brune WH; Hunter JF; Kroll JH; Cummings MJ; Brogan JF; Parmar Y; Worsnop DR; et al. Effect of oxidant concentration, exposure time, and seed particles on secondary organic aerosol chemical composition and yield. Atmos. Chem. Phys 2015, 15, 3063–3075.

(44). Ng NL; Chhabra PS; Chan AWH; Surratt JD; Kroll JH; Kwan AJ; McCabe DC; Wennberg PO; Sorooshian A; Murphy SM; et al. Effect of NO_x level on secondary organic aerosol (SOA) formation from the photooxidation of terpenes. Atmos. Chem. Phys 2007, 7, 5159–5174.

(45). Charrier JG; Richards-Henderson NK; Bein KJ; McFall AS; Wexler AS; Anastasio C Oxidant production from source-oriented particulate matter-part 1: Oxidative potential using the dithiothreitol (DTT) assay. Atmos. Chem. Phys 2015, 15, 2327–2340.

(46). Charrier J; Anastasio C On dithiothreitol (DTT) as a measure of oxidative potential for ambient particles: evidence for the importance of soluble transition metals. Atmos. Chem. Phys. Discuss 2012, 12, 11317–11350.

(47). Chen JY; Jiang H; Chen SJ; Cullen C; Ahmed CMS; Lin Y-H Characterization of electrophilicity and oxidative potential of atmospheric carbonyls. Environ. Sci.: Processes Impacts 2019, 21, 856–866.

(48). Lin Y-H; Arashiro M; Clapp PW; Cui T; Sexton KG; Vizuete W; Gold A; Jaspers I; Fry RC; Surratt JD Gene expression profiling in human lung cells exposed to isoprene-derived secondary organic aerosol. Environ. Sci. Technol 2017, 51, 8166–8175. [PubMed: 28636383]

(49). Reuter S; Gupta SC; Chaturvedi MM; Aggarwal BB Oxidative stress, inflammation, and cancer: how are they linked? Free Radicals Biol. Med 2010, 49, 1603–1616.

(50). Letavayová L; Vlčková V; Brozmanová J Selenium: From cancer prevention to DNA damage. Toxicology 2006, 227, 1–14. [PubMed: 16935405]

(51). Kung CP; Murphy ME The role of the p53 tumor suppressor in metabolism and diabetes. J. Endocrinol 2016, 231, R61–R75. [PubMed: 27613337]

(52). Rodin SN; Rodin AS Human lung cancer and p53: the interplay between mutagenesis and selection. Proc. Natl. Acad. Sci. U.S.A 2000, 97, 12244–12249. [PubMed: 11035769]

(53). Levine AJ; Oren M The first 30 years of p53: Growing ever more complex. Nat. Rev. Cancer 2009, 9, 749. [PubMed: 19776744]

(54). Hu W; Feng Z; Levine AJ The regulation of multiple p53 stress responses is mediated through MDM2. Genes Cancer 2012, 3, 199–208. [PubMed: 23150753]

(55). Puzio-Kuter AM The role of p53 in metabolic regulation. Genes Cancer 2011, 2, 385–391. [PubMed: 21779507]

(56). Wu GS The functional interactions between the MAPK and p53 signaling pathways. Cancer Biol. Ther 2004, 3, 156–161. [PubMed: 14764989]

(57). Gupta A; Shah K; Oza MJ; Behl T Reactivation of p53 gene by MDM2 inhibitors: A novel therapy for cancer treatment. Biomed. Pharmacother 2019, 109, 484–492. [PubMed: 30551517]

(58). Steinbrenner H; Speckmann B; Pinto A; Sies H High selenium intake and increased diabetes risk: Experimental evidence for interplay between selenium and carbohydrate metabolism. J. Clin. Biochem. Nutr 2011, 48, 40–45. [PubMed: 21297910]

(59). Ong SH; Hadari YR; Gotoh N; Guy GR; Schlessinger J; Lax I Stimulation of phosphatidylinositol 3-kinase by fibroblast growth factor receptors is mediated by coordinated recruitment of multiple docking proteins. Proc. Natl. Acad. Sci. U.S.A 2001, 98, 6074–6079. [PubMed: 11353842]

(60). Chen Z; Trotman LC; Shaffer D; Lin H-K; Dotan ZA; Niki M; Koutcher JA; Scher HI; Ludwig T; Gerald W; Cordon-Cardo C; Paolo Pandolfi P Crucial role of p53-dependent cellular senescence in suppression of Pten-deficient tumorigenesis. Nature 2005, 436, 725–730. [PubMed: 16079851]

(61). Webster NJG; Resnik JL; Reichart DB; Strauss B; Haas M; Seely BL Repression of the insulin receptor promoter by the tumor suppressor gene product p53: a possible mechanism for receptor overexpression in breast cancer. Cancer Res 1996, 56, 2781–2788. [PubMed: 8665514]

(62). Burns J; Manda G Metabolic pathways of the warburg effect in health and disease: Perspectives of choice, chain or chance. Int. J. Mol. Sci 2017, 18, No. 2755.

(63). Seki T; Kumagai T; Kwansa-Bentum B; Furushima-Shimogawara R; Anyan WK; Miyazawa Y; Iwakura Y; Ohta N Interleukin-4 (IL-4) and IL-13 suppress excessive neutrophil infiltration and hepatocyte damage during acute murine schistosomiasis japonica. Infect. Immun 2012, 80, 159–168. [PubMed: 22038918]

(64). Hazari YM; Bashir A; Habib M; Bashir S; Habib H; Qasim MA; Shah NN; Haq E; Teckman J; Fazili KM Alpha-1-antitrypsin deficiency: Genetic variations, clinical manifestations and therapeutic interventions. Mutat. Res., Rev. Mutat. Res 2017, 773, 14–25.

(65). Kagan P; Sultan M; Tachlytski I; Safran M; Ben-Ari Z Both MAPK and STAT3 signal transduction pathways are necessary for IL-6-dependent hepatic stellate cells activation. PLoS One 2017, 12, No. e0176173. [PubMed: 28472150]

(66). Junttila IS Tuning the cytokine responses: An update on interleukin (IL)-4 and IL-13 receptor complexes. Front. Immunol 2018, 9, No. 888. [PubMed: 29930549]

(67). Gour N; Wills-Karp M IL-4 and IL-13 signaling in allergic airway disease. Cytokine 2015, 75, 68–78. [PubMed: 26070934]

(68). Hao Y; Kuang Z; Jing J; Miao J; Mei LY; Lee RJ; Kim S; Choe S; Krause DC; Lau GW Mycoplasma pneumoniae modulates STAT3-STAT6/EGFR-FOXA2 signaling to induce overexpression of airway mucins. Infect. Immun 2014, 82, 5246–5255. [PubMed: 25287927]

(69). Crosby LM; Waters CM Epithelial repair mechanisms in the lung. Am. J. Physiol.: Lung Cell. Mol. Physiol 2010, 298, L715–L731. [PubMed: 20363851]

(70). Jiang H; Ahmed C; Canchola A; Chen JY; Lin Y-H Use of dithiothreitol assay to evaluate the oxidative potential of atmospheric aerosols. Atmosphere 2019, 10, No. 571.

(71). Lin M; Yu JZ Dithiothreitol (DTT) concentration effect and its implications on the applicability of DTT assay to evaluate the oxidative potential of atmospheric aerosol samples. Environ. Pollut 2019, 251, 938–944. [PubMed: 31234260]

(72). De Santiago A; Longo AF; Ingall ED; Diaz JM; King LE; Lai B; Weber RJ; Russell AG; Oakes M Characterization of selenium in ambient aerosols and primary emission sources. Environ. Sci. Technol 2014, 48, 8988–8994. [PubMed: 25075640]

(73). Lin Z-Q; Cervinka V; Pickering IJ; Zayed A; Terry N Managing selenium-contaminated agricultural drainage water by the integrated on-farm drainage management system: role of selenium volatilization. Water Res 2002, 36, 3150–3160. [PubMed: 12171414]

(74). Lin ZQ; Schemenauer RS; Cervinka V; Zayed A; Lee A; Terry N Selenium volatilization from a soil-plant system for the remediation of contaminated water and soil in the San Joaquin Valley. J. Environ. Qual 2000, 29, 1048–1056.

(75). Karlson U; Frankenberger WT; Spencer WF Physicochemical properties of dimethyl selenide and dimethyl diselenide. J. Chem. Eng. Data 1994, 39, 608–610.

(76). Karlson U; Frankenberger WT Determination of gaseous selenium-75 evolved from soil. Soil Sci. Soc. Am. J 1988, 52, 678–681.

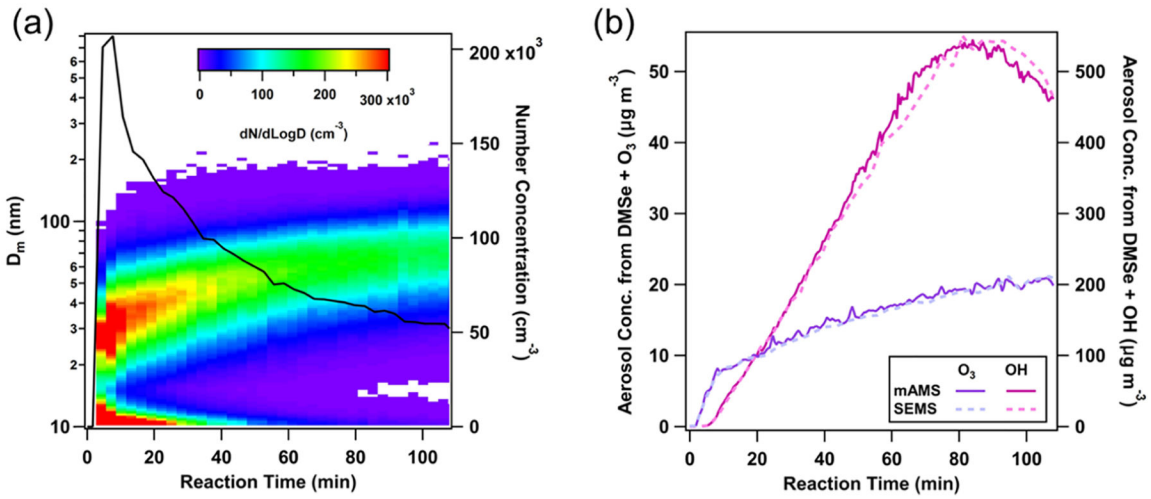

Figure 1.

(a) Nucleation and growth of DMSe-derived SOA particles during O_3 oxidation of DMSe; (b) aerosol mass concentrations during OH and O_3 oxidation experiments, as determined by mAMS and SEMS; aerosol density values of 1.8 and 1.6 g cm^{-3} were used in O_3 and OH oxidation experiments, respectively.

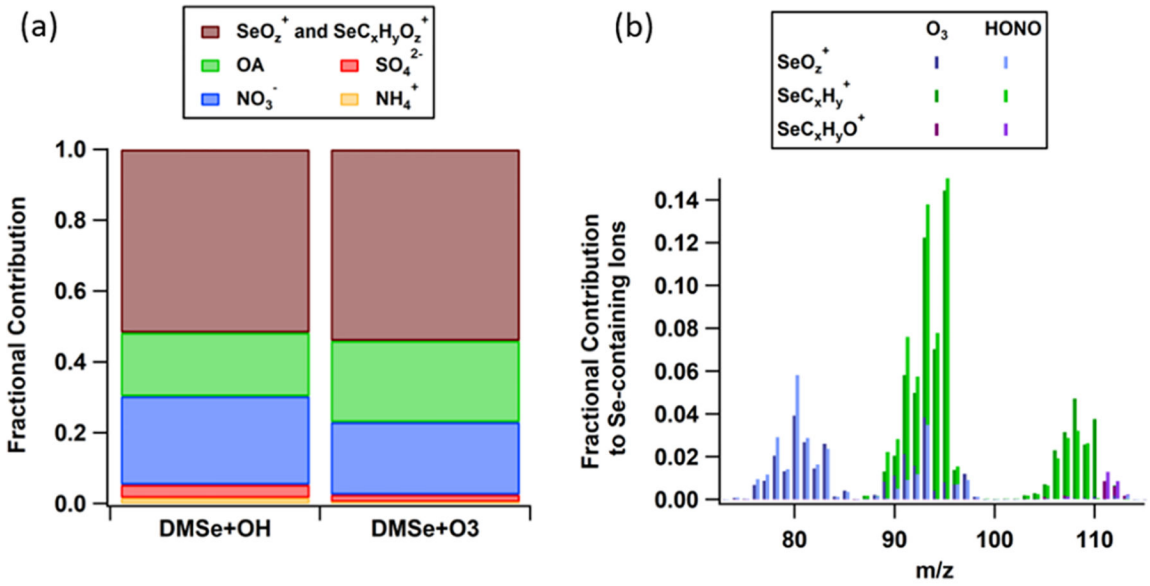

Figure 2.

(a) Fractional contribution of SOA species to total SOA mass during filter collection. (b) Average high-resolution mass spectrometry (HR-MS) analysis of Se-containing fragments during the peak mass concentration of O_3 and OH oxidation experiments. Frequency of each atom in the designated ions is specified by integers *x*, *y*, and *z*.

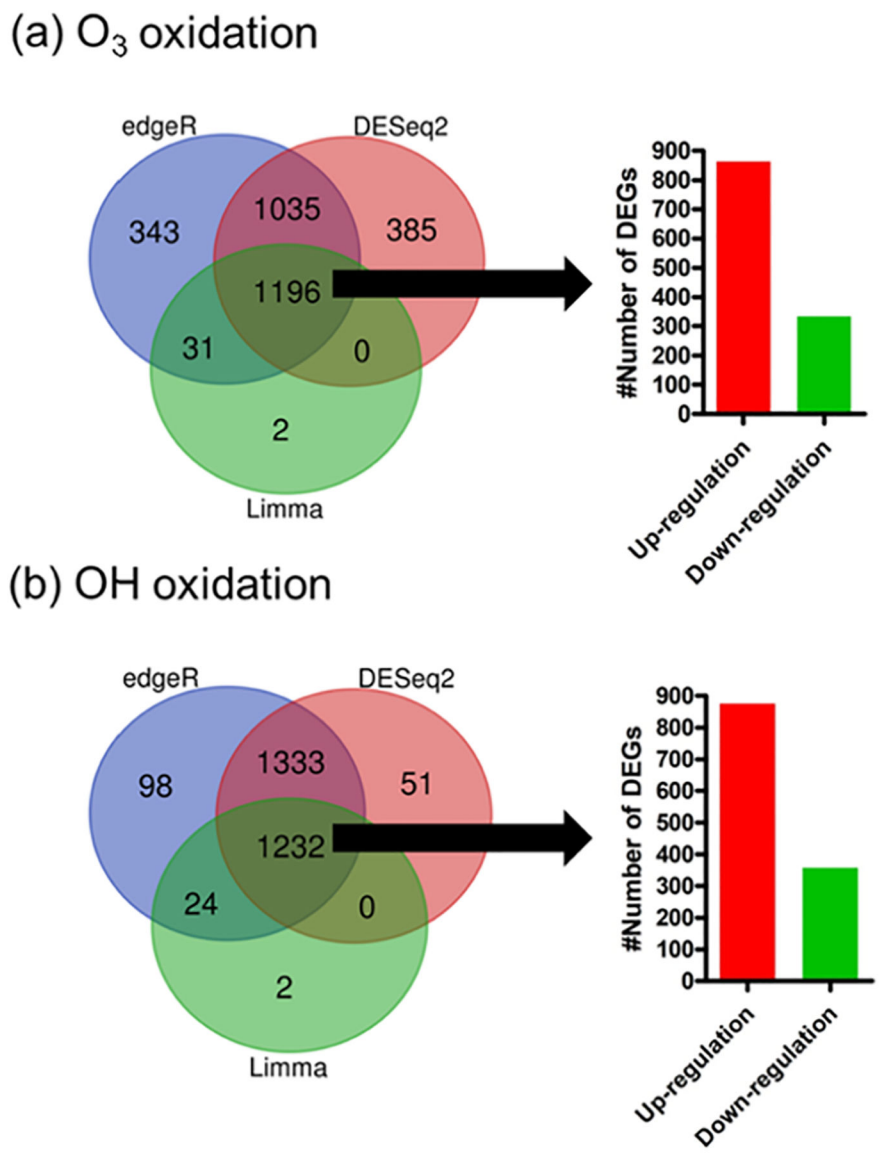

Figure 3.

DEGs identified from three different tools, including DESeq. 2, edgeR, and Limma for BEAS-2B cells exposed to DMSe-derived SOA resulting from (a) O_3- and (b) OH-initiated oxidations. Sorting criteria: Log_2 FC |±1|, *p* value = 0.01, FDR/adjusted *p* value =0.01, and CPM ≥ 1. Bar graphs represent the number of upregulated and downregulated DEGs in the intersections of three gene set inputs from DESeq. 2, edgeR, and Limma.

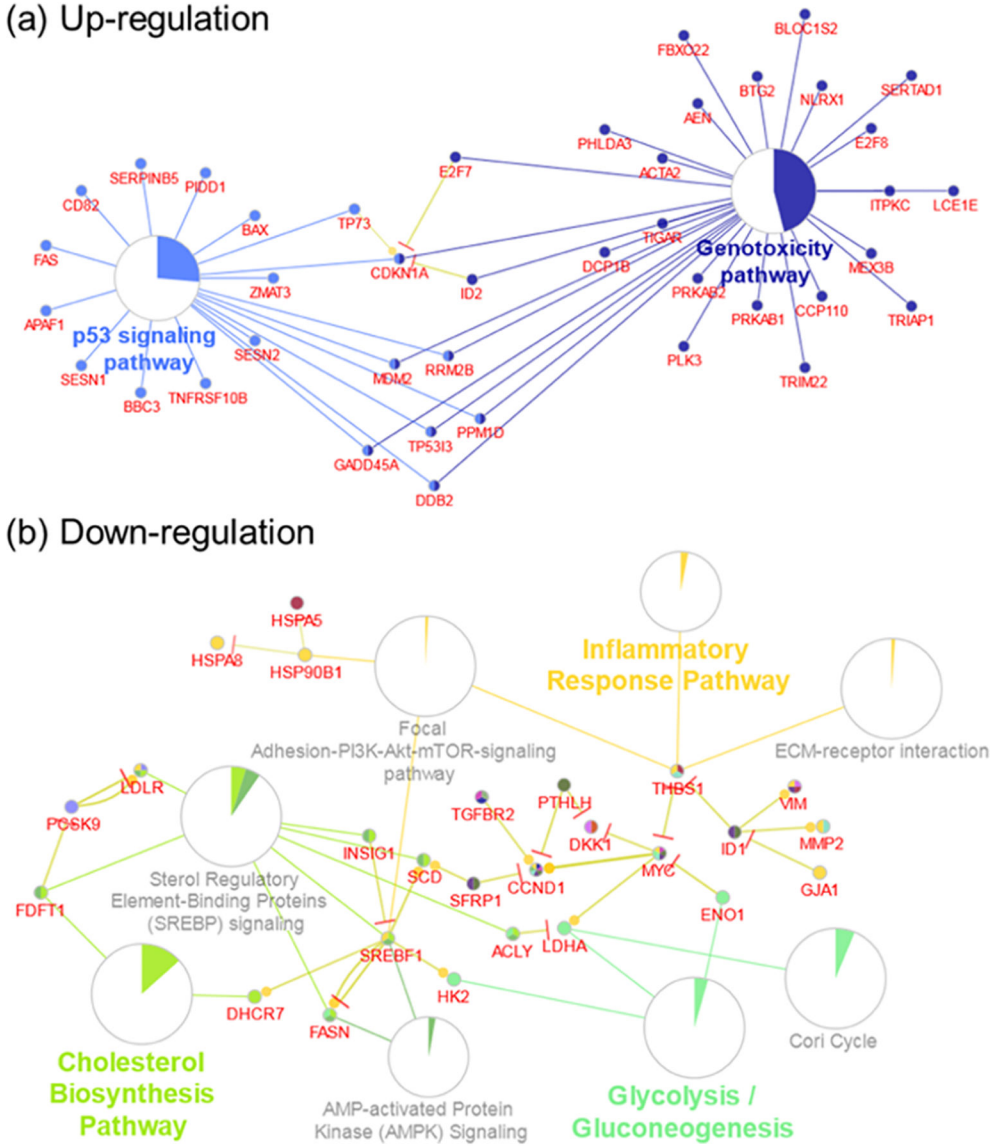

Figure 4.

Major biological pathways enriched for (a) upregulated and (b) downregulated DEGs, FDR < 0.01. Pie charts represent the percentage of visible genes of a pathway. Genes shared between pathways are shown.